Supporting Information

On-demand Coupling of Electrically Generated Excitons with Surface Plasmons via Voltage-Controlled Emission Zone Position

Yuriy Zakharko,[†] Martin Held,[†] Fabrizio-Zagros Sadafi,[‡] Florentina Gannott,[†]Ali Mahdavi,[§] Ulf Peschel,[§,#] Robin N. Klupp Taylor,[‡] and Jana Zaumseil*[,†]

[†] Institute for Physical Chemistry, Universität Heidelberg, D-69120 Heidelberg, Germany

[‡] Institute of Particle Technology (LFG), Friedrich-Alexander-Universität Erlangen-Nürnberg, D-91058 Erlangen, Germany

[§] Institute of Optics, Information and Photonics and Graduate School in Advanced Optical Technologies, Friedrich-Alexander-Universität Erlangen-Nürnberg, D-91054 Erlangen, Germany

[#] Institute of Condensed Matter Theory and Solid State Optics, D-07743 Jena, Germany

1. Methods

Nanorod synthesis and ligand exchange

Nominally 70×20 (130×20) nm gold nanorods (NRs) were synthesized following the method reported by Ye *et al.*[1] Seeds were prepared by mixing 5 ml of 0.5 mM $HAuCl_4$ with 5 ml of 0.2 M cetyltrimethylammonium bromide (CTAB) in a 25 ml round bottom flask. 0.6 ml of freshly prepared 0.01 M $NaBH_4$ were diluted to 1 ml and injected into the flask under vigorous stirring. The solution color changed rapidly from yellow to brown and stirring was stopped after 2 minutes. The solution was aged for 30 minutes to ensure complete $NaBH_4$ consumption. 9 g of CTAB and 1.234 g of sodium oleate were dissolved in water at 50 °C and the solution was left to cool down to 30 °C. Subsequently, 12 (24) ml of a 4 mM $AgNO_3$ solution were added and the solution was gently stirred for 15 minutes. Then, 250 ml of 1 mM $HAuCl_4$ were added and the solution turned form yellow to colorless after 90 seconds of stirring. 2.1 (3) ml of 37 % HCl were introduced during gentle stirring and after another 15 minutes 1.25 ml of 0.064 M ascorbic acid were injected under vigorous stirring. After 30 seconds the 0.8 (0.05) ml of the as-prepared seed solution were introduced to the reaction solution, which was stirred for another 30 seconds. Finally, the dispersion was left undisturbed at 30 °C overnight in order to allow NR growth.

For the ligand exchange procedure the following method was used as described elsewhere.[2] Briefly, under vigorous stirring, equal volumes of gold NRs dispersion in water (washed 3 times) and a polyethyleneglycol-thiol (PEG-SH) solution (1 mg/mL in H_2O) were mixed, sonicated for 30 sec and left to react for 12 h. Excess PEG molecules were removed by centrifugation at 15000 rpm for 10 min and the PEGylated nanorods were redispersed in tetrahydrofuran (THF).

LEFET fabrication

Light-emitting field-effect transistors (LEFETs) were fabricated in bottom-contact, top-gate geometry. Gold NRs were doctor-bladed from the THF dispersion onto glass substrates (Schott AF32 Eco) with pre-patterned titanium alignment markers. The PEG-SH ligand was then removed

by oxygen plasma treatment. The nanorod layer was photolithographically patterned using double-layer photoresist (LOR5B/S1813) and etching with KI/I_2 solution. A 1 nm layer of aluminum was evaporated on top and oxidized in air in order to electrically insulate the NRs. Photolithographically patterned source-drain electrodes (lift-off, 2 nm Cr / 30 nm, W/L = 25, L = 20 μm) were aligned with respect to the edge of the nanorod layer. No decrease in NRs density was observed during the lift-off step.

The semiconducting polymer DPPT-BT (2,5-*bis*(2-octyldodecyl)-3,6-di(thiophen-2-yl) diketopyrrolo[3,4-*c*]pyrrole-1,4-dione-*alt*-benzo*[c]*[1,2,5]thiadiazole, M_n = 33 kg mol^{-1}, M_w = 87 kg mol^{-1}, purchased from Flexink Ltd.) was spincoated from a 8 mg ml^{-1} chlorobenzene solution at 5000 rpm for 60 s and annealed at 200 °C for 30 min. A film thickness of 15 nm was determined by profilometry. A 11 nm thin layer of PMMA (syndiotactic poly(methyl methacrylate), Polymer Source, M_w = 350 kg mol^{-1}, 6 mg ml^{-1} in n-butylacetate) was obtained by spincoating at 6000 rpm for 60 s and annealed at 80 °C for 30 min. A layer of 38 nm HfO_x was deposited on top by atomic layer deposition (Ultratech Savannah S100), using tetrakis(diemethylamino)hafnium (TDMAH) as the precursor and H_2O as the oxygen source, 300 cycles at 100 °C). Shadow mask evaporation of 35 nm of silver as the gate electrode completed the device. All processing steps were carried out in a dry-nitrogen glovebox.

Characterization

SEM images of the gold nanorods were recorded with a Carl Zeiss Auriga field-emission scanning electron microscope at 1 kV. The anisotropic complex refractive index of DPPT-BT copolymer was measured with a Horiba Jobin Yvon UVISEL ellipsometer and fitted with DeltePsi 2 software. Current-voltage characteristics were recorded with an Agilent 4156C Semiconductor Parameter Analyzer or a Keithley 2612A source meter. Gate dielectric capacitances were determined with an Agilent E4980A Precision LCR Meter. Absorption spectra of DPPT-BT thin films and gold NRs were recorded with a Cary 6000i UV/Vis/NIR absorption spectrometer (Varian). Extinction spectra of the gold NRs within the devices were calculated from white light transmission through the regions with (T_{NRs}) and without (T_{ref}) NRs defined as: 1-(T_{NRs}/T_{ref}). Electroluminescence (EL) images were recorded with a thermoelectrically cooled 256 × 360 pixel InGaAs camera (Xenics XEVA-CL-TE3, 800 – 1600 nm). The emission was collected through a near-infrared objective (Olympus LCPLN50XIR ×50, NA 0.65 with correction collar). An Acton SpectraPro SP2358 spectrometer (grating 150 lines/mm) and a liquid nitrogen-cooled InGaAs line camera (PI Acton OMA V:1024 1.7) was used to record EL spectra. All spectra were corrected against the response of the detection system with a calibrated tungsten halogen lamp.

For photoluminescence (PL) intensity maps a diode laser at 785 nm (Alphalas GmbH) operating in a pulsed (< 60 ps, 10 MHz repetition rate) mode was used for excitation. Samples were mounted on a piezo-stage (Mad City Labs Inc.) and illuminated with a focused beam through a ×100 near-IR, 0.8 N.A. objective. Emitted photons were collected with the same objective and detected by an InGaAs/InP single-photon avalanche diode (Micro Photon Devices, Italy) directly or after wavelength separation with a Cornerstone 260 monochromator. Intensity/photon counts correction was applied to account for the detector operating in gated mode with 30 μs hold-off time. PL intensity maps were acquired for the entire detection range (900-1600 nm) by raster-scanning with a piezo-stage at a step size of 0.5 μm. PL spectra were measured at 11 different positions to average inhomogeneities of the sample.

2. Results

A. Characterization of synthesized gold NRs

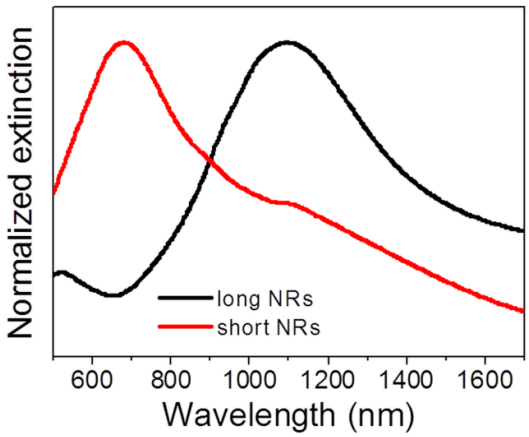

Figure S1. Extinction spectra of short (70×20 nm) and long (130×20 nm) NRs on a glass substrate.

B. 3D Finite-difference time-domain calculations

3D finite-difference time-domain (FDTD) simulations were performed using commercial software (FDTD Solution v8.12.527, Lumerical Solutions Inc., Canada). A uniform mesh size of 1.5 nm (X, Y and Z-directions) was used in the region with a steep variation of the dielectric function (X×Y×Z=490×490×90 nm^3 around gold NR). Outside of these regions the grid was defined by the auto non-uniform mesh technique. The optical constants of gold were taken from Johnson and Christy.[3] The complex dielectric constants of the DPPT-BT polymer were acquired from ellipsometry measurements (Figure S2a). Following Zhang *et al.* for a similar DPPT-TT copolymer, anisotropy in the Z-direction was added (n_z=1.55 and k_z=0) to take into account the in-plane (XY) orientation of the polymer chains.[4] The dispersion curves of the polymer were fitted by a multi-coefficient model over the spectral range from 500 nm to 1500 nm.

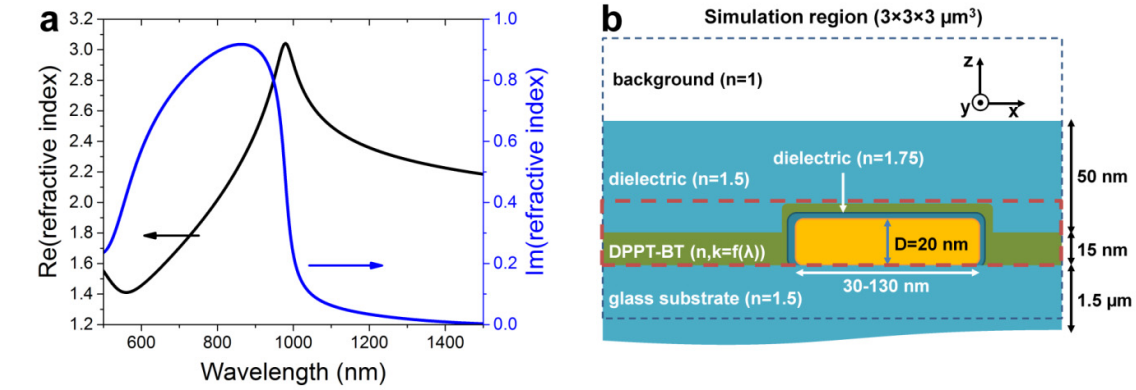

Figure S2. (a) Real and imaginary parts of complex refractive index of DPPT-BT copolymer. (b) Schematic layout of the 3D-FDTD calculations.

The schematic layout of the simulation region (boundaries defined by perfectly matched layers) is depicted in Figure S2b, including the glass substrate, a thin (1 nm) AlO_x and a thin (h=15 nm) DPPT-BT layer covering gold NRs (D=20 nm) with variable length (L=30-130 nm) and 50 nm of gate dielectric layer. To reduce computational resources and computational time, we took advantage of the symmetric/antisymmetric boundary conditions. A plane wave polarized along the long or short axis (X or Y direction) of the NR was launched at different angles of incidence (0-50°) to the substrate, to calculate wavelength-dependent extinction spectra of the gold NR (Figure S3), and record electromagnetic fields with a 3D monitor (X×Y×Z=300×300×30 nm^3, red dashed line in Figure S2b) set around gold NR. Field intensity enhancement $|E_x/E_0|^2$ and thus radiative decay rate enhancement[5] (as shown in Figure 2b of the main text) was calculated by averaging values from the 3D monitor excluding values of cells/positions not representing DPPT-BT copolymer and dividing by the values of the structure without gold NRs. The emitting dipoles randomly oriented with respect to the gold NR (in XY plane, as the copolymer backbone) can be represented as the superposition of two orthogonal dipoles, i.e. X- and Y-polarized. Therefore, orientation-averaged enhancement factor can be simplified to the average of those two values, where enhancement factor for Y-polarized dipole is negligible, i.e. ~1.

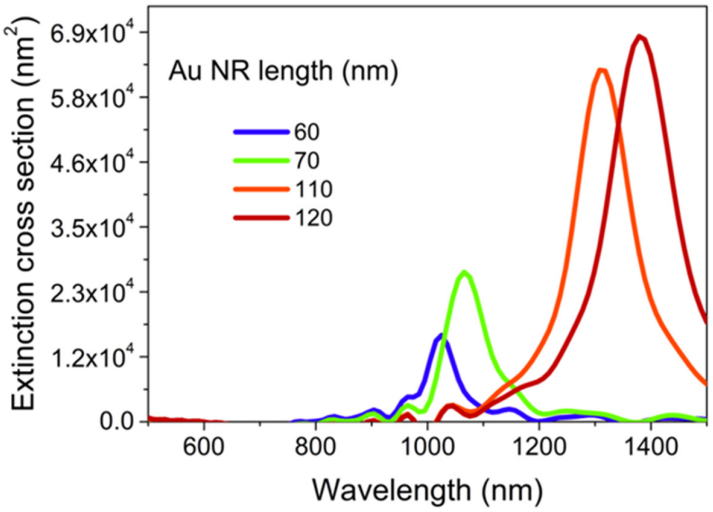

Figure S3. Extinction cross section of a single gold NR (D=20 nm) for different lengths (L=60, 70, 110 and 120 nm) illuminated with light polarized along the long axis of the NR. For non-polarized light the extinction is halved.

Role of the metal-related losses for emission enhancement

For distances of few nanometers to the surface of the gold nanorod emitting dipoles suffer from nonradiative relaxation due to the losses in the metallic structures. In order to verify that these losses are insignificant compared to the internal losses of the semiconducting layer (with PL quantum yield ~0.01 %) we performed simulations of the emitting dipoles for two polarizations with respect to the 100×20 nm gold NR and at different distances from the NR surface (see Figure S4 for the simulation layout). A uniform mesh size of 0.1 nm (X, Y and Z-directions) was used around the emitting dipole (X×Y×Z=5×5×5 nm^3). We simplified the simulations layout with respect to that in Figure S2b in order to take advantage of the symmetric/antisymmetric boundary conditions of the simulation region and to be able to perform near-to-far-field transformation (discussed in the next section). Test simulations confirmed that these changes did not influence obtained results noticeably (not shown here). Calculating the radiated power (and thus normalized radiative decay rate) by the dipole into the far-field (red dashed line representing corresponding power monitor in Figure S4) and comparing it with the power dissipated by the dipole (i.e. total decay rate; red dotted line), one can easily calculate radiative, nonradiative decay rates and quantum

efficiencies for different configurations. Typically this approach is used for a homogeneous lossless medium and rather straightforward. In the present case, dipoles are located in the absorbing semiconducting layer (i.e. non zero absorption at the emission wavelength).

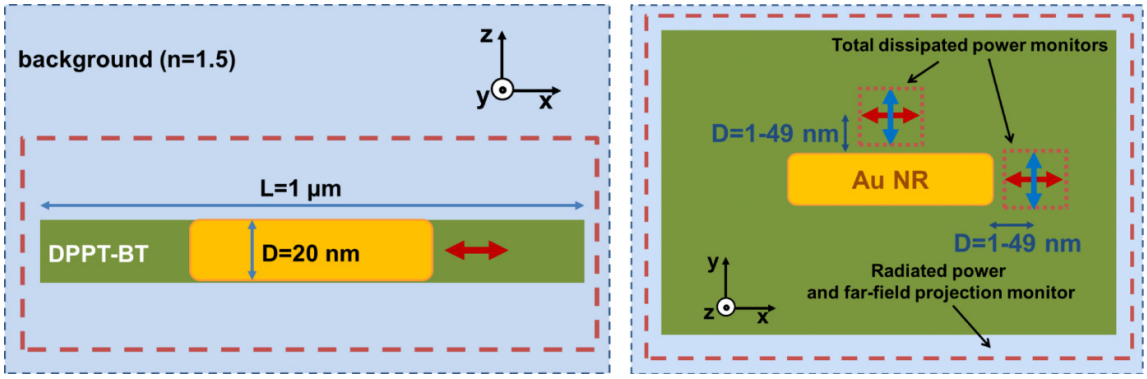

Figure S4. Schematic layout of the 3D-FDTD calculations with the dipole emitter (indicated as the red/blue double-sided arrows for two polarizations and configurations with respect to the gold NR). Red dashed lines indicate power/field profile monitors.

For this reason, power dissipated by the dipole (proportional to the total decay rate K^0_{tot}) even without gold NR include the radiative component (K^0_{rad}) as well as some absorptive nonradiative losses due to the polymer itself (K^0_{abs}):

$$K^0_{tot} = K^0_{rad} + K^0_{abs} \quad (1)$$

In this type of simulations intrinsic emission quantum efficiency (η_0) is not taken into account. In order to do so, the real total decay rate K'_{tot} (i.e. experimentally measurable) can be represented as the sum of the radiative decay rate and nonradiative decay K^0_{nrad} (physically including both absorptive losses of the polymer environment and additional nonradiative recombination channels that are not accountable by the simulations).

$$K'_{tot} = K^0_{rad} + K^0_{nrad} = {K^0_{rad}}/{\eta_0} \quad (2)$$

Here, decay rates are normalized to have the same normalized radiative decay rate (K^0_{rad}) as in Equation 1.

After introducing the gold NR into the system, the new simulated total decay rate (K_{tot}) is higher due to the additional metal quenching (K_{nrad}), while radiative decay rate (K_{rad}) increases due to the Purcell effect:

$$K_{tot} = K_{rad} + K_{abs}^{0} + K_{nrad} \quad (3)$$

Combining Equations 1-3, we obtain the ratio of the nonradiative losses introduced by the gold NR to the intrinsic losses of the emitting dipole:

$$K_{nrad}/K_{nrad}^{0} = \frac{K_{tot} - K_{tot}^{0} + K_{rad}^{0} - K_{rad}}{K_{rad}^{0}(1/\eta_0 - 1)} \quad (4)$$

Obviously, the final emission quantum efficiency of the dipole close to the gold NR depends on this ratio and the radiative decay enhancement ($F = K_{rad}/K_{rad}^{0}$):

$$\eta = \frac{K_{rad}}{K_{rad} + K_{nrad}^{0} + K_{nrad}} = \frac{K_{rad}}{K_{rad} + K_{nrad}^{0}(1 + K_{nrad}/K_{nrad}^{0})} = \frac{F}{F + (1/\eta_0 - 1)(1 + K_{nrad}/K_{nrad}^{0})} \quad (5)$$

This equation once again highlights the fact that for maximum quantum efficiency one would need to increase radiative decay enhancement and decrease metal losses.

Calculated values of the radiative decay enhancement, ratio of the metal-related to intrinsic polymer losses (Equation 4) and quantum efficiency enhancement at the plasmon resonance for 100×20 nm gold NR and different NR-dipole configurations (variable 1-49 nm dipole to surface distance at the center and NR end, see Figure S4 for layout) are shown in Figure S5.

One can clearly see in Figure S5a that the maximum radiative decay enhancement (up to 250 times) is observed when the distance is small and when the dipole is located at the NR end where the local fields are most intense and for polarization along the NR long axis. For other configurations (NR center) local fields are not that strong. Interestingly, for a dipole at the NR end and polarized perpendicularly to the long axis local fields are even lower, forcing the radiative decay rate to decrease ~180 times.

As for the metal related losses (Figure S5b), they are only comparable (at most) to the intrinsic losses of the DPPT-BT polymer at very close proximity of the emitting dipole to the gold NR. Beyond the few nanometers region around the NR these losses are negligible, i.e. below few percent of the intrinsic losses (approximate precision of the simulations indicated by the shaded region in Figure S5b). Therefore, the emission quantum efficiency enhancement (Figure S5c) follows the same trends as the radiative decay enhancement while the absolute values are at most halved.

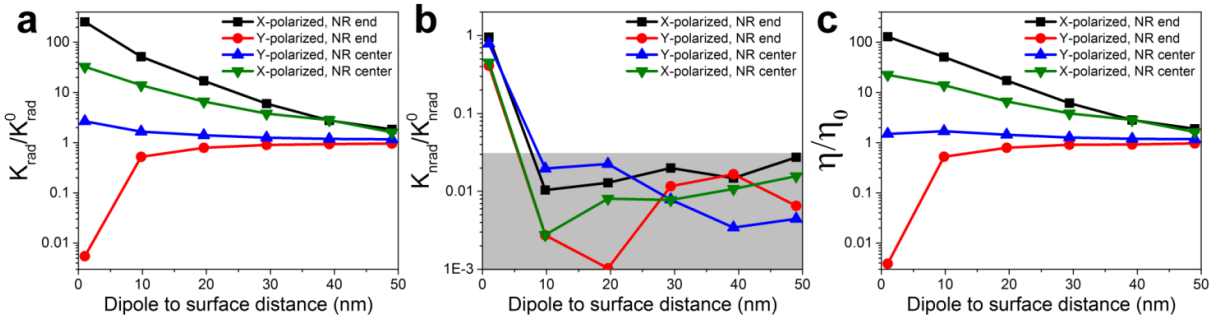

Figure S5. (a) Radiative decay enhancement, (b) ratio of metal-related to intrinsic polymer losses and (c) quantum efficiency enhancement at plasmon resonance as a function of the dipole distance to the surface of the gold NR (100×20 nm) for two polarizations of the dipole with respect to the long axis of the NR (at the center and NR end, see Figure S4 for layout). Intrinsic emission quantum efficiency of the dipole is $\eta_0 = 0.0001$.

Light outcoupling/collection enhancement considerations

In order to estimate possible contributions of the outcoupling/scattering of the light guided/trapped in the DPPT-BT layer by the gold NRs, we performed additional simulations of an emitting dipole in the layer with a similar layout as in Figure S2b, but without the gold nanorod. The amount of power propagating through the YZ and XZ planes (X and Y directions, respectively) was calculated from corresponding surface monitors located 100 nm from the dipole. Less than 10 % of the power at the emission wavelengths (1000-1500 nm) propagating in these directions propagates within the polymer layer. In other words, even for a very high nanorod density of 100 NRs/μm^2 only 10 % of the energy could possibly be scattered by the NRs. These considerations are qualitatively justified by the fact that the emitting dipoles are oriented in the XY plane (the transition dipoles are along the

polymer chains, which are predominantly lying flat within the thin spincoated film), and thus only a small fraction of power can be trapped in a thin (15 nm) polymer layer.

The simulations of the volume-averaged field enhancement calculated for the different angles of incidence of the plane wave (0-50°) for 100×20 nm gold NR (at plasmon resonance) also show that enhancement of the power emitted at the corresponding angle should deviate by less than 3 % compared to the enhancement for the normal direction of emission (Figure S6). From this, we can conclude that for the collection angle of the objectives used in PL/EL experiments gold NRs on average do not change emission patterns and thus collection efficiency noticeably.

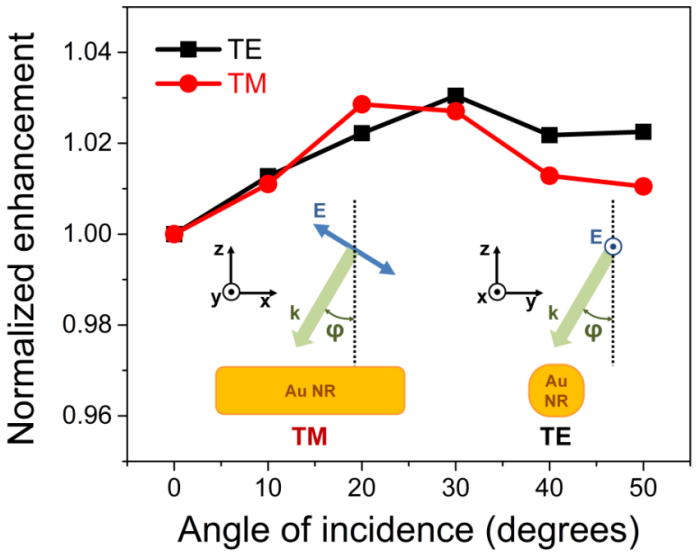

Figure S6. Normalized volume-averaged local field enhancement factors at the plasmon resonance of 100×20 nm NR for different angles of incidence of the plane wave. Inset shows relative orientations of the polarization and propagation direction of the plane wave with respect to the long axis of NR.

This observation seems to contradict common knowledge that gold NRs should change the emission pattern of the dipoles close to the NRs. In order to elaborate on this aspect, we performed near-to-far-field transformation of the radiated power by the dipole with the use of field profile monitors surrounding the structure (red dashed line in Figure S4) for different NR-dipole configuration (the same as in the previous section, i.e. various polarizations, distances, etc.). Comparing far-field

emission patterns with and without 100×20 nm gold NR we obtained a far-field emission enhancement plot (at plasmon resonance), or in other words, angle dependent emission enhancement factors as show in Figure S7. Let us first focus on the emission enhancement pattern for the configuration with the maximum enhancement, i.e. when emitting dipole is oriented along the long axis of the gold NR and is located at its end (Figure S7a). One can clearly see that the gold NRs does change the emission pattern towards positive X-values even at rather large distances. For example for the 1 nm separation enhancement factors at 52° and 308° (corresponding to the collection angles of the objective and power propagating along Z-axis, i.e. towards objective) are ~280 and ~230, respectively. However, due to symmetry, these values will be swapped for the dipole located at the opposite end of the NR. Taking into account two opposite dipoles the averaged value (280+230)/2=255 is close to the average 254-fold enhancement at 0°. In other words, two dipoles located on the opposite ends of the NR almost cancel out emission pattern changes induced by the NR. As for the other separations, the situation is similar, e.g. for the 49 nm distance, opposite dipoles averaging at 52°/308° gives 1.97-fold enhancement versus 1.76 at 0°. For the remaining configurations of the dipoles, we again can see a change of emission pattern of the dipoles when collected by the objective (i.e. along Z-axis) but it is also compensated by the dipoles located on the opposite ends of the NR.

The only exception is the dipole located 1 nm from the NR end, but polarized along the short axis of the NR (Figure S7b, f, j). However, in this case, the changed emission pattern will not contribute significantly to the overall optical response since as shown in the previous section, this dipole configuration has low radiative decay rate and large nonradiative losses.

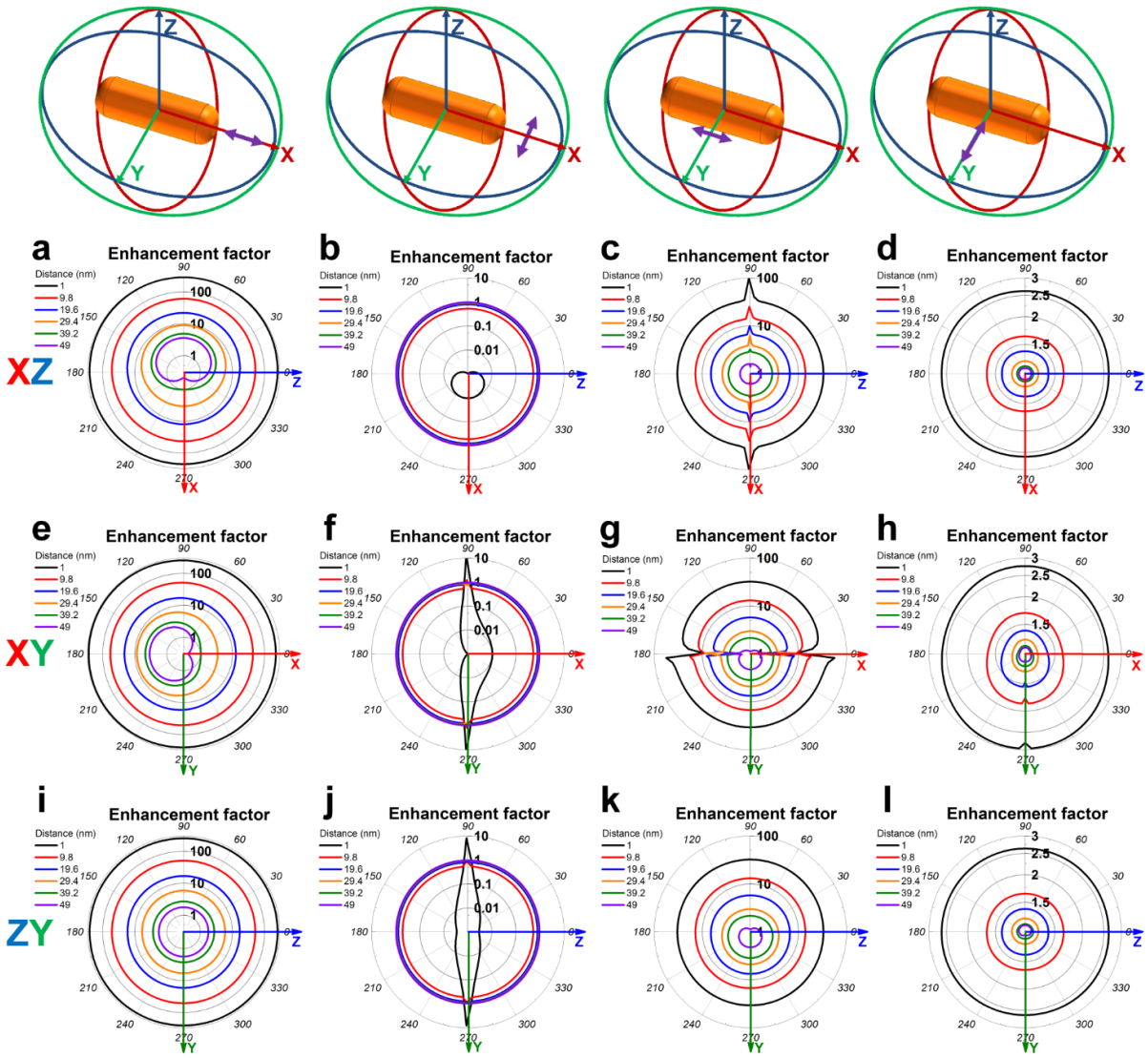

Figure S7. Top: schematic of the relative orientation of the emitting dipole located in XY-plane (purple double-sided arrow) with respect to the 100×20 nm gold NR. Corresponding angle-dependent (far-field) emission enhancement factor plots as a function of the NR-dipole separation (from 1 to 49 nm) for XZ (a-d), XY (e-h) and ZY (i-l) planes.

Local emission enhancement

Observed plasmon-enhanced EL intensity (I) is a sum of light emission from polymer emitters oriented perpendicularly ($I_\perp$) and parallel ($I_\parallel$) to the gold NRs:

$$I = I_\perp + I_\parallel = \frac{I_0}{2} F_\perp + \frac{I_0}{2} F_\parallel \quad (6)$$

, where I_0 is EL intensity without gold NRs, $F_\perp$ and $F_\parallel$ are volume-averaged EL enhancement factors for two orthogonal relative orientations of emitting dipoles and gold NRs. Since there is no enhancement for perpendicular orientation, we can set $\mathbf{F_\perp=1}$. Further, only small fraction of the DPPT-BT emitters are enhanced close to the gold NRs with a factor F_{local}. Since NRs are located in a plane, this fraction can be defined as the ratio of the field confinement area (S_{conf}) around gold NR to a surface area of polymer per single NR (S_0, i.e. inverse of the surface density of gold NRs). The remaining fraction of the polymer (S_0-S_{conf})/S_0 is not enhanced, i.e. $\mathbf{F_0=1}$. As the result, EL enhancement factor for parallel-oriented dipoles-NRs $F_\parallel$ is:

$$F_\parallel = \frac{S_{conf}}{S_0} F_{local} + \frac{S_0 - S_{conf}}{S_0} F_0 \quad (7)$$

The enhancement factors (F_{obs}) shown in Figure 4d, h of the main text can be defined by dividing Equation 6 by **I** and including Equation 7 as follows:

$$F_{obs} = \frac{I}{I_0} = \left(\frac{S_{conf}}{S_0} F_{local} + \frac{S_0 - S_{conf}}{S_0} F_0 + 1\right)/2 \quad (8)$$

This yields the following expression for the local enhancement factor F_{local}:

$$F_{local} = 2(F_{obs} - 1)\frac{S_0}{S_{conf}} + 1 \quad (9)$$

The confinement area as a value of in-plane (XY) field confinement in thin DPPT-BT layer can be defined, for example, as the statistical measure of the effective mode volume[6] divided by the height over which averaging of field intensity variations needs to be performed (Z direction):

$$S_{conf} = \frac{1}{h}\frac{(\int E(r)\,dV)^2}{\int E(r)^2\,dV} \quad (10)$$

, where E(r) is the electromagnetic energy density taking into account the electric and magnetic fields. Integration should be performed over a volume large enough to let the fields decay, or in our case, it is done over a whole 3D field monitor, i.e. 300×300×30 nm^3 region (around gold NR defined as the red dashed line in Figure S2b). As one can see from field intensity distribution (XZ plane) around 100×20 nm gold NR at plasmon resonance (Figure S8a), rather small integration volume (h=30 nm) is sufficient to estimate characteristic XY field confinement in DPPT-BT layer. Calculated values of the field confinement area for different lengths of gold NR are shown in Figure S8b. In addition, the calculated footprint of the gold NR depicted as the dotted lines indicates that the field confinement area is mostly influenced by the field concentrated outside the NR.

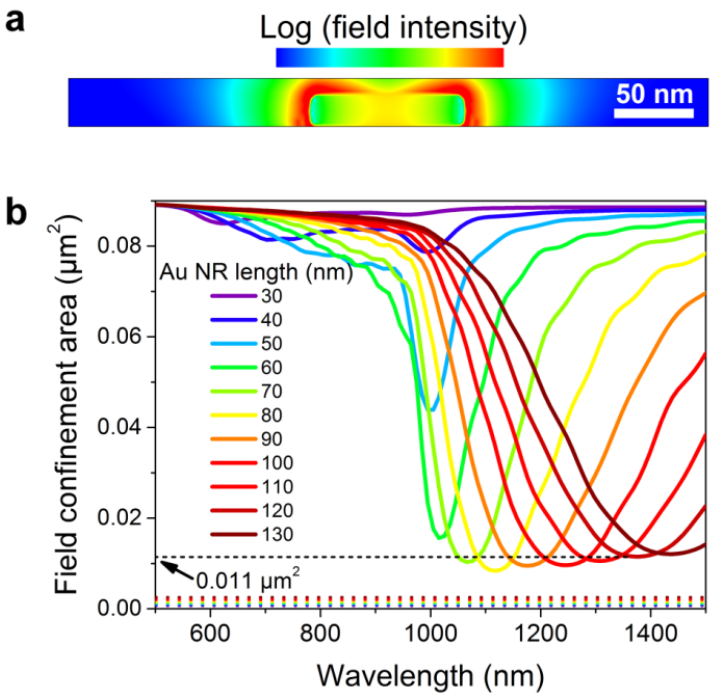

Figure S8. (a) Field intensity distribution around gold NR (100×20 nm) at plasmon resonance (XZ plane, simulation layout as in Figure S2b). (b) Field confinement area for gold NRs (D=20 nm) with different length (L=30-130 nm). Corresponding footprints of the NRs are indicated as the dotted lines.

By combining the obtained values for short and long NRs: the confinement area (~0.011 μm^2), density of NRs aligned parallel to the emitting dipoles (half of the density of all NRs, i.e. 15.9 μm^{-2} and 6.9 μm^{-2}, respectively) and EL enhancement factors in Figure 4 of the main text, we obtain the following local EL enhancement values:

$F_{local,\ short\ NRs}$(at 1100 nm)= 2×(2-1)/(0.011×15.9)+1 ≈ **12**

$F_{local,\ long\ NRs}$(at 1350 nm)= 2×(2.75-1)/(0.011×6.9)+1 ≈ **47**

C. Transport characteristics of LEFETs

The transfer curves for channels with short and long NRs shown in Figure S10 indicate a clear ambipolar behavior with the typical V-shape at high drain voltages. In contrast to the constant current sweeps (Figure 4a, e) EL emission changes in intensity as it moves through the channel.

The device parameters (mobility, threshold voltages, see Table S12) of LEFETs with and without nanorods are similar with slightly lower field-effect mobilities for transistors with nanorods, which might be due to increased surface roughness. The higher currents for devices with long nanorods may be explained by improved charge injection at the electrodes (*i.e.* electric field-enhancement at nanorod tips protruding from the electrode edges) as indicated by the output characteristics (S11) at low drain voltages.

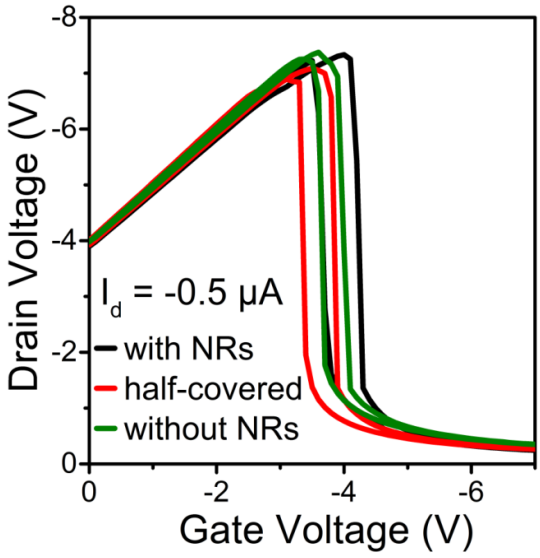

Figure S9. Gate voltage sweeps at constant drain current for LEFETs without, half-covered and with gold NRs.

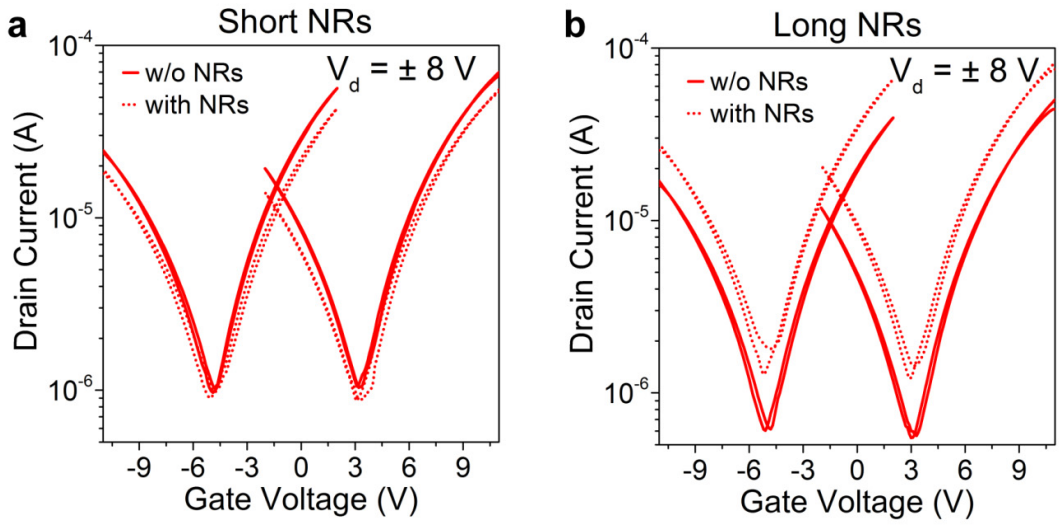

Figure S10. Ambipolar transfer characteristics of LEFETs with (a) short and (b) long gold NRs within the channel and corresponding LEFETs without any NRs.

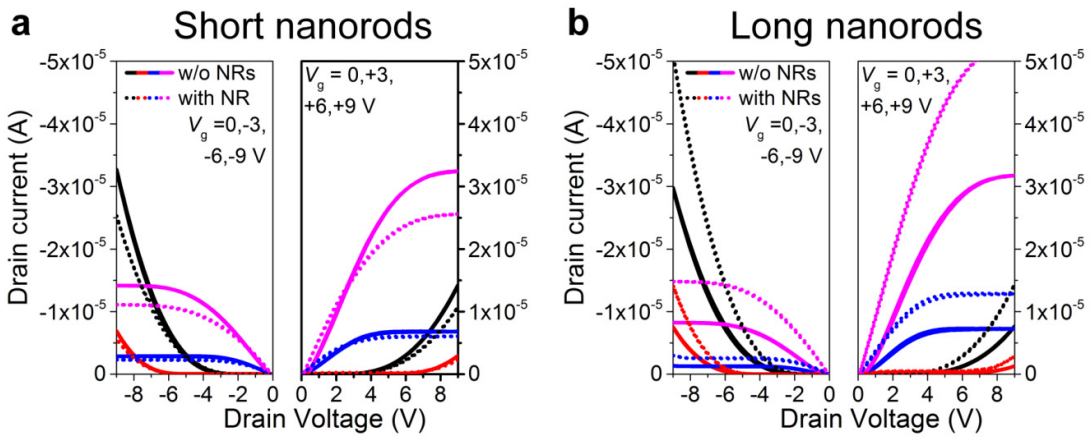

Figure S11. Ambipolar output characteristics of LEFETs fabricated with (a) short and (b) long gold NRs and corresponding channels without NRs.

Table S12. Charge transport parameters (saturation mobility μ_{sat} and threshold voltages V_{Th} for holes and electrons) extracted from FETs with and without gold nanorods in the channel and with half-covered channels.

	$\mu_{sat,h}$ ($cm^2V^{-1}s^{-1}$)	$V_{Th\ sat,h}$ (V)	$\mu_{sat,e}$ ($cm^2V^{-1}s^{-1}$)	$V_{Th\ sat,e}$ (V)
Fully covered with short NRs	0.21 ± 0.06	-4.0 ± 0.9	0.49 ± 0.15	2.8 ± 0.7
Half-covered with short NRs	0.30 ± 0.08	-4.1 ± 0.6	0.63 ± 0.22	2.8 ± 0.5
Without NRs	0.29 ± 0.07	-3.9 ± 0.3	0.63 ± 0.20	2.8 ± 0.3
Fully covered with long NRs	0.29 ± 0.05	-4.3 ± 0.3	0.61 ± 0.08	2.9 ± 0.4
Half- covered with long NRs	0.36 ± 0.04	-4.1 ± 0.3	0.79 ± 0.09	2.8 ± 0.4
Without NRs	0.36 ± 0.03	-4.0 ± 0.2	0.81 ± 0.05	2.7 ± 0.4

D. Videos of the moving emission zone in LEFET half-covered with short and long gold NRs

Near-infrared videos (wavelengths 800−1600 nm) of the recombination and emission zone from a LEFET channel half-covered with **short** gold NRs during a gate voltage sweep from -4.3 V to −2.6 V, and with **long** gold NR during a gate voltage sweep from -4.5 V to −3.9 V each at a constant drain current (I_d = −0.5 μA). One voltage step (2 mV) per frame and an integration time of 5 seconds were used. In order to exclude apparent broadening of the emission zone, a reference measurement with three frames for each gate voltage step (*i.e.* oversampling) was performed and did not show any difference.

1) **LEFET_short_NRs.avi**
2) **LEFET_long_NRs.avi**

E. Electroluminescence spectra with and without gold NRs

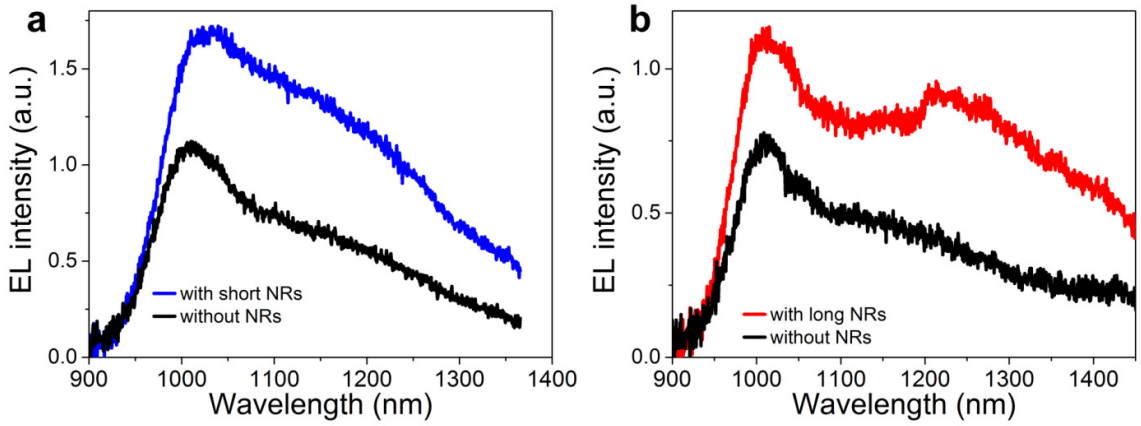

Figure S13. Electroluminescence spectra with emission zone coupled to short (a) and long (b) NRs in comparison to emission from channel area without NRs.

References

(1) Ye, X.; Zheng, C.; Chen, J.; Gao, Y.; Murray, C. B. Using Binary Surfactant Mixtures To Simultaneously Improve the Dimensional Tunability and Monodispersity in the Seeded Growth of Gold Nanorods. *Nano Lett.* **2013**, *13* (2), 765–771.

(2) Thierry, B.; Ng, J.; Krieg, T.; Griesser, H. J. A Robust Procedure for the Functionalization of Gold Nanorods and Noble Metal Nanoparticles. *Chem. Commun.* **2009**, *1* (13), 1724–1726.

(3) Johnson, P. B.; Christy, R. W. Optical Constants of the Noble Metals. *Phys. Rev. B*. **1972**, *6*, 4370–4379.

(4) Zhang, X.; Richter, L. J.; DeLongchamp, D. M.; Kline, R. J.; Hammond, M. R.; McCulloch, I.; Heeney, M.; Ashraf, R. S.; Smith, J. N.; Anthopoulos, T. D.; Schroeder, B.; Geerts, Y. H.; Fischer, D. A.; Toney, M. F. Molecular Packing of High-Mobility Diketo Pyrrolo-Pyrrole Polymer Semiconductors with Branched Alkyl Side Chains. *J. Am. Chem. Soc.* **2011**, *133* (38), 15073–15084.

(5) Biteen, J. S.; Sweatlock, L. A.; Mertens, H.; Lewis, N. S.; Polman, A.; Atwater, H. A. Plasmon-Enhanced Photoluminescence of Silicon Quantum Dots: Simulation and Experiment. *J. Phys. Chem. C* **2007**, *111* (36), 13372–13377.

(6) Oulton, R. F.; Bartal, G.; Pile, D. F. P.; Zhang, X. Confinement and Propagation Characteristics of Subwavelength Plasmonic Modes. *New J. Phys.* **2008**, *10* (10), 105018.